Available online at www.sciencedirect.com

ScienceDirect

Procedia Structural Integrity 28 (2020) 2228–2234

Structural Integrity Procedia

www.elsevier.com/locate/procedia

1st Virtual European Conference on Fracture

Flexible graphite as beam dumping material in the TDE blocks of the Large Hadron Collider

E. Solfiti[a], M. Calviani[b], A. Perillo-Marcone[b], J.M. Heredia[b], C. Torregrosa[b], A. Alvaro[c], F. Berto[a]

[a]*Department of Mechanical and Industrial Engineering, Norwegian University of Science and Technology, Richard Birkelands vei 2B, Trondheim, 7491, Norway*

[b]*CERN, Geneva, Switzerland*

[c]*Department of Material and Nanotechnology, SINTEF Industry, Trondheim, Norway*

Abstract

The Large Hadron Collider (LHC) is a high energy particle collider at the European Laboratory for Particle Physics (CERN) in Geneva, Switzerland. The LHC Beam Dumping System (LBDS) is composed by different equipment employed to extract and absorb the LHC circulating beam in case of need. At the end of the LBDS resides the LHC main dump (so called TDE, which stands for Target Dump External). The TDE block is constituted by several graphite blocks with different densities enclosed in a 318L stainless steel jacket. Among the different type of carbon-based materials, the flexible graphite is the one owning the lowest density (1–1.2 g/cm^3). It differs from typical graphite forms such as polycrystalline and pyrolytic graphite in that no binder is added during the production process. The bonding frictional forces due to particle asperities give the typical flexibility to the material and contribute to the deformation mechanism. In order to predict the thermo-mechanical response to the proton beam-induced sudden energy deposition, the material behavior needs to be investigated in–depth in a wide range of temperature and strain–rates. In this preliminary work, the static properties of a commercial flexible graphite (Sigraflex® from SGL Carbon) have been observed at room temperature in the in–plane direction. Two sides DIC technique has been employed in order to get a reliable measurement of the strain on both front and edge specimen surfaces; the crosshead displacement–rate was varied between 0.01–10 mm/min. Finally, a discussion about the stress–strain behavior and the deformation mechanism has been given.

Keywords: Flexible graphite; DIC; static properties;

* E. Solfiti Tel.: +39 3405863109
E-mail address: emanuele.solfiti@ntnu.no

10.1016/j.prostr.2020.11.051

1. Introduction

The Large Hadron Collider (LHC) is the largest and most powerful particle accelerator in the world (CERN website). It is located in Geneva (Switzerland) in a 27 km length circular ring and is part of the bigger CERN's accelerator complex (see Fig.1(a)). Two circular pipes are hosted in a tunnel where two 6.5 TeV/c counter rotating proton beams are make to collide at 13 TeV center of mass. Each 6.5 TeV/c beam (expected to be ramp up to 7 TeV/c over the next few years) is composed of several bunches (currently 2748) with a pulse intensity of up to $1.2 \cdot 10^{11}$ particles per bunch (expected to be increased up to $1.8 \cdot 10^{11}$ particles per bunch by 2024). The amount of energy achievable during the impact is the sum of the colliding beam energies and is limited by both the radius of the facility and the strength of the magnets that keep the particles in the circular orbit. LHC is an hadronic machine, namely capable of accelerating and colliding hadrons, such as protons and ions. The two counter-rotating beams are made to collider in four different locations along the ring, each one corresponding to a different experiment facility and, whenever requested, they are extracted out of the trajectory by a set of magnets and eventually dumped in the Target Dump External (TDE) blocks, i.e. the external dump systems highlighted in the magnification circle of Fig.1(a). The beams coming from both directions are deviated from the circular orbit into special tangent tunnels with a length of 700 metres each. The final block of each tunnel is the only item able to withstand the impact of the full beam: it is made of horizontally stacked graphite blocks of different densities (SGL Carbon Sigrafine® R7300, Sigrafine® HLM and Sigraflex® with respective densities of 1.73 g/cm^3, 1.72 g/cm^3 and 1.1-1.2 g/cm^3), shrink fitted into a sealed steel vessel with 7734 mm length (length of the core), 700 mm in radius, 12 mm in thickness and filled with nitrogen in order to keep inert atmosphere (see Fig.1(b)). The beam penetrates along the graphite core and as a result of the beam-matter interaction phenomenon, it produces high levels of energy density deposition. A set of four horizontal (MKBH) and six vertical (MKBV) dilution fast-pulsed kickers is used to sweep the beam in a kind of spiral-like trajectory in order to dilute the deposited energy in the core. Further details about this system can be found in several sources such as Schmidt et al. (2006). The lowest density part emphasized in Fig.1(b) is made of 1650 Sigraflex® sheets with 2 mm thickness and density equals to 1.1-1.2 g/cm^3. They are stacked together, constrained at the two ends with two extruded graphite disks (Sigrafine® HLM) and two snap rings so that only contact forces can act among them. The deposited energy peak occurs inside this volume where the temperature reaches 1500°C (even up to 2000°C in case of failure of 2 MKBH units) in a time interval typically equals to 90μs. At a first approximation, it can be assumed that this process occurs in quasi instantaneous heating conditions where the specific energy deposited and the maximum temperature are related by the simplified form of the Fourier heat equation: $\dot{q} = \rho\, c_p\, \frac{\partial T}{\partial t}$. In this case, the density, the specific heat and the thermal conductivity dependence on temperature should be known in order to solve the thermal problem and find the maximum temperature achievable. Further in depth, it should be considered that the material expands naturally, depending on the temperature increase itself. Such expansion occurs so suddenly that the region surrounding the impacted volume does not manage to heat up due to its own thermal inertia and prevents such expansion. This phenomenon gives rise to high pressures that, in the worst cases, can originate the propagation of stress waves (Martin et al. (2019, 2016); Bertarelli et al. (2013, 2008); Scapin (2013); Zukas (1990)). The problem is therefore coupled with both mechanical and thermal aspects. Sigraflex® sheets play a fundamental role in such a system, but the knowledge about their constitutive behavior and thermophysical properties, especially in the high temperature range, is still inadequate and mostly related to its more common commercial applications. This material belongs to the group of flexible graphite: it shows good resilience and viscous response due to its particular microstructure (Gu et al. (2002); Luo and Chung (2000)) resulting well-exploitable in sealing applications and gaskets often in sandwiched structures with stainless steel foils or in the form of impregnated yarns (some examples on SGL Carbon Website). It is obtained by uniaxial or rolling compression of expanded graphite particles without any additive binder (Shane et al. (1968)) and the result is a porous anisotropic material that retains some similarities with the more common types of graphite, such as polycrystalline and pyrolytic graphite but differs in terms of micro-scale morphology and mechanical strength (Solfiti and Berto (2020a)). The high thermal and electrical conductivity, conformability, capability of dissipate energy, chemical resistance up to beyond 2500°C and low gas permeability, make it also effective as thermal interface material for cooling and insulation, where the low weight and volume are of crucial importance (see Solfiti and Berto (2020b) and Chung (2016) for a more complete review on the applications). In terms of mechanical properties instead, the out-of-plane compression and the in-plane tension behavior at room temperature were the most investigated fields. Dowell and Howard (1986) set the first milestones on this part of research, also reporting some data at very high tem-

perature. Some recent works moved the investigation in static compression and recovery loading at room temperature (Toda et al. (2013); Kobayashi et al. (2012)), also observing how the deformation units behave upon the external load application. The use of Sigraflex® in the LHC external dumps, can be considered as a unique application and lays out of the commercial ones listed above. This means that an extension of the investigation upon a wider range of temperature and strain-rates is requested, with the purpose of predicting the behavior and improving the suitability in the current and future TDE design conditions. Indeed the High Luminosity Large Hadron Collider (HL-LHC), that is the future update of LHC whose first run is planned for 2027, is being designed to achieve a larger beam intensity (Apollinari et al. (2017)). In this collaboration between CERN and NTNU, a first exploratory investigation is performed on Sigraflex® specimens regarding their static tensile properties at room temperature in the in-plane direction, in order to approach the material, to understand the requested experimental techniques and therefore establish a starting point for a wider testing campaign.

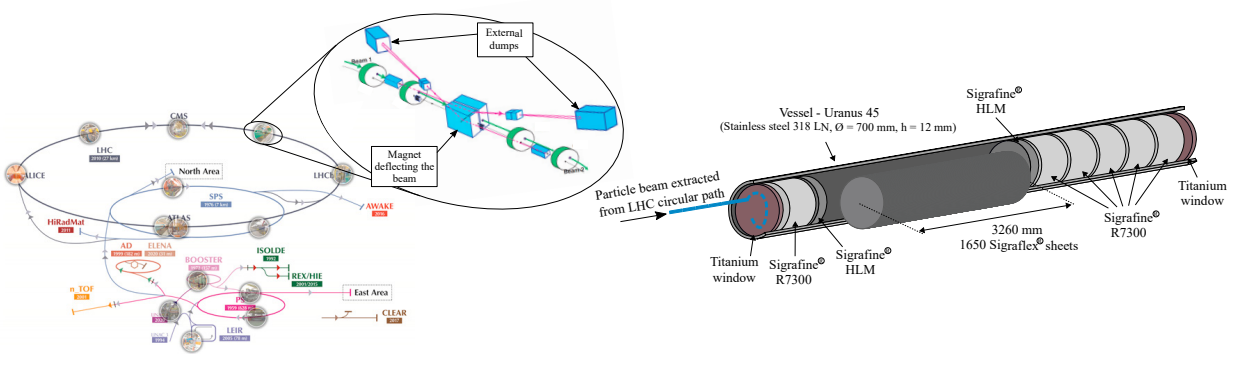

(a) (b)

Fig. 1: (a) Large Hadron Collider facility overview (CERN website) and external beam dumps or TDE blocks (picture reworked from Schmidt et al. (2006)) and (b) TDE graphitic core (section view).

2. Materials and methods

Despite its softness, the procedure to obtain flexible graphite specimens should be carefully chosen in order to get a sufficient surface refinement. A rolled foil of Sigraflex® L20010C, whose properties are reported in Table 1, was provided by SGL Carbon. The waterjet CNC machine WJS NCH 30 was chosen for the cutting procedure and the following parameters were found to give the better results: jet pressure = 3800 bar, beam diameter = 0.3 mm and sand GRIT = 230. The Sigraflex® foils as delivered and the specimen geometry are shown in Fig. 3(a) and (b). No polishing or further machining was worked out on the specimens.

Size	$1000 \times 1000 \times 2$ mm
Density	1 g/cm^3
Tensile strength	> 4 MPa
Ash content	≤ 0.15 %
Elongation at break	> 1 %
Specific heat (20°C)	0.7 J/(Kg K)
Coeff. of thermal expansion (20 - 1000°C)	1×10^{-6}K^{-1} (in - plane), 30×10^{-6}K^{-1} (out - of - plane)
Thermal stability	- 250 to + 3000°C (up to + 400°C in presence of oxygen)

Table 1: Sigraflex® L20010C foils properties as reported in SGL Carbon website.

The tensile static tests were performed in a MTS Exceed® Universal testing machine with 5 kN load cell. A batch of four specimen couples was chosen upon four different crosshead displacement rates as reported in Fig. 3(a).

Fig. 2: (a) Sigraflex® foils as delivered with magnification view and (b) specimen geometry and dimensions [mm].

The displacement and load were recorded from the machine embodied LVDT and load cell, respectively. Two-sides DIC recording technique was used in order to get an accurate description of the specimen deformation. A front view (width surface) and a side view (thickness surface) were captured at the same time as illustrated in Fig. 3(b). Since the material originally showed shiny surfaces, a fine painting pattern was found to be necessary in both the width and thickness edges. Moreover, the strain from DIC recordings was calculated from two different gauge lengths: the first one, which will be referred to as the full gauge length, corresponds to the standard and commonly used gauge length (32 mm). The second one is calculated between the upper and lower bounds of the fracture surrounding region that is arbitrarily chosen around the fracture in each case. The latter one will be referred to as the short gauge length and can reach a few millimetres in length (Fig. 3(b)).

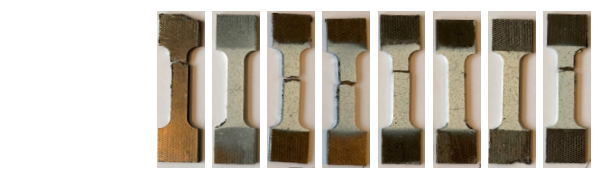

	1	2	3	4	5	6	7	8
Displacement rate [mm/s]	0.01		0.1		1		10	
Strain rate [s^{-1}]	$3.125 \cdot 10^{-4}$		$3.125 \cdot 10^{-3}$		$3.125 \cdot 10^{-2}$		$3.125 \cdot 10^{-1}$	

(a)

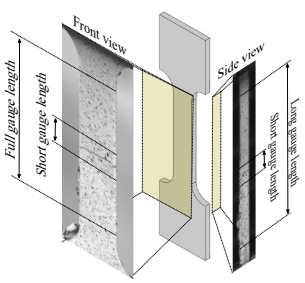

(b)

Fig. 3: (a) Tested specimens visual summary and (b) DIC investigated views with an examples of the considered gauge lengths.

3. Results and discussion

The static curves are plotted in Fig.4. The curves for displacement rate equal to 10 mm/min were found to be undersampled from the DIC camera and are only reported in terms of crosshead displacement in Fig.4(a). In Fig.4(b)-(d) some combinations of static curves are compared upon different recorded views and gauge lengths. The failures occurred with brittle behaviors and were located on the specimen free length despite the high level of anisotropy and porosity of flexible graphite. The failures appears brittle without occurrence of yielding and a typical in-plane layer delamination seems to be the main fracture mechanism. In some cases, the DIC camera at the wide edge side could not detect the first crack location because it grew among the inner layers giving some evidences only either on the thin edge side or on the opposite wide edge side. Therefore, only the DIC camera placed on the thin edge side could always detect the first fracture location. However, the static curves plotted with the displacements from both sides look

similar. Also the static curves calculated with both the full and short gauge lengths are well overlapped confirming that the material does not have a strong deformation gradient along the longitudinal direction until the fracture occurs. The behavior of the stress-strain curve is similar to that of polycrystalline graphite. This was discussed in Jenkins (1962) in which a simple power-law model such as $\varepsilon = A\sigma + B\sigma^2$ was proposed for the theoretical compression behavior of pure crystalline graphite. In Dowell and Howard (1986) such relation was also proposed for flexible graphite in tensile static conditions. It fitted the stress-strain curve up to approximately a half of the ultimate tensile strength and this was also confirmed in this work: typical values for the reciprocals of A and B coefficients were obtained by means of non linear least-square regression algorithm and were found to be equal to A^{-1}= 0.59 GPa and B^{-1} = 0.51 GPa, respectively. Since flexible graphite is made by compression of expanded graphite flakes, the microstructure can be observed at least upon two magnification scales. The first one corresponds to the micro-scale, in which the deformation units play the most important role on the load carrying mechanism. The crack grows across the boundaries also from multiple locations (Gu et al. (2002)) and determines the main contribution to the overall deformation. The second one achieves the micro-sheets level. The micro-sheets or micro-disks result from compression of the worms cell walls (nanometric scale, Chung (2014)) and, assuming that their behavior is similar to that of pure graphite, it is proposed that the load carrying mechanism at the very beginning of load application would be lead by the micro-sheets deformation, whereas the sliding of deformation units would take place at higher load levels. Despite this would explain the deviation in the constitutive behavior from the pure graphite theoretical behavior, a more detailed investigation is requested to clarify and confirm such hypothesis. The presence of a linear region in the stress-strain behavior is questionable; taking the chord slope in the 0.01 and 0.1 mm/min tests, (from $\varepsilon = 0\,\%$ to approximately $\varepsilon = 0.4\,\%$ that corresponds to 1.1 - 1.2 MPa), it results the elastic modulus to be equal to 1.35 - 2.45 GPa. Such values agree with that reported in Xi and Chung (2019) and appears one order of magnitude lower than the elastic modulus in the out-of-plane compression given in Dowell and Howard (1986) and in Neograf Solutions for a similar commercial flexible graphite. No marked

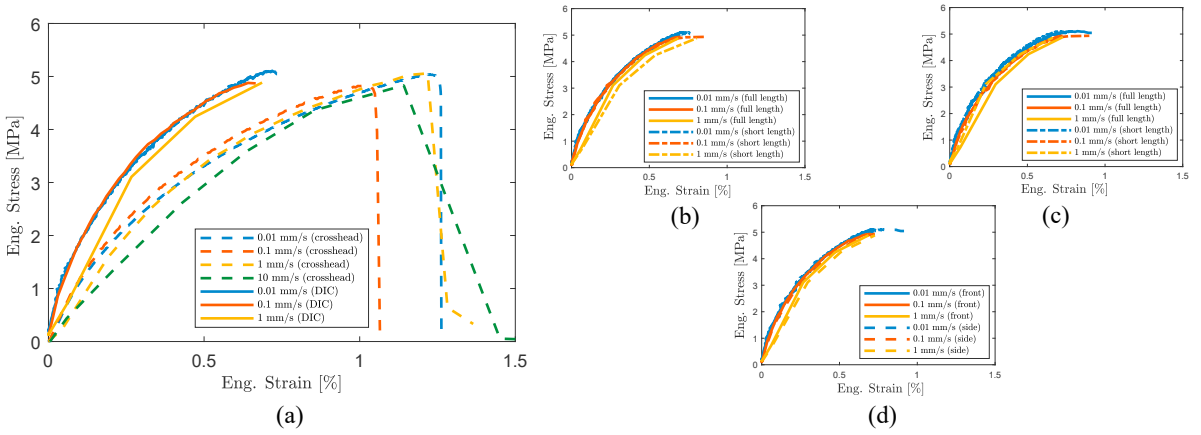

Fig. 4: Static curves: (a) front view, full length; (b) front view, full length and short length; (c) side view, full length and short length; (d) full length, front view and side view.

trend is noticeable in Fig.5 where the ultimate tensile stress and the strain at maximum stress are reported against the strain-rate. The tensile strength and the strain at break, taken as the average of all the experimental data, are equal to $\simeq$ 5 MPa and 0.8%, in agreement with values reported from the other sources (Dowell and Howard (1986); SGL Carbon).

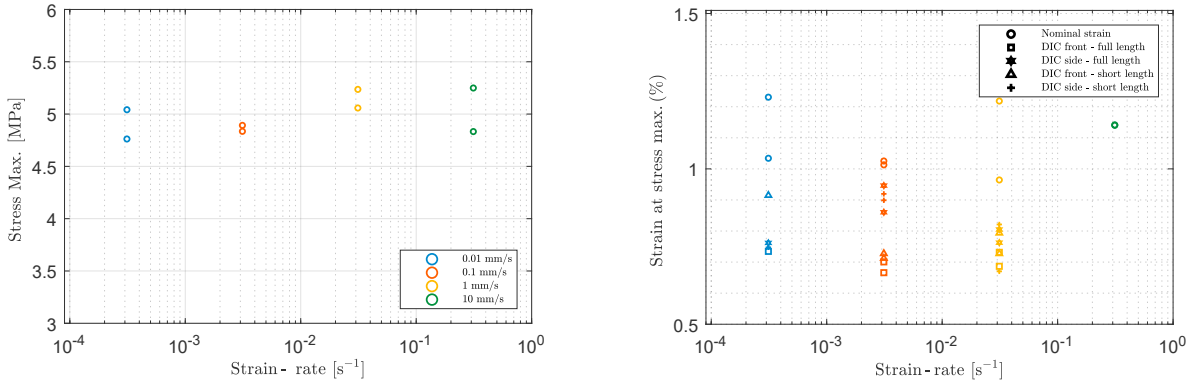

Fig. 5: (a) UTS and (b) strain at maximum stress dependence on strain - rate.

4. Conclusion

The static properties of Sigraflex® were investigated upon four different displacement rates. The strain was recorded accurately by means of two side DIC camera technique, essential to capture the early crack growth location. The main conclusion can be summarized in the following points:

- the unidimensional stress-strain behavior appears as that of a brittle material. The curve is not linear since the early beginning, in analogy with polycrystalline graphite typical curves, showing a downward concavity in the whole domain, without occurrence of yielding. All the specimens were broken at maximum stress. No difference were noticed neither between the strain measured in the front and side edge surfaces nor in the strain measured in the long and short gauge length. The fracture surfaces shows typical brittle aspect and the macroscopical fracture mechanism seems to be the delamination (or sliding) of flatten units in the in-plane direction that coincides with the load direction. It is finally proposed that the contribution to the deformation mechanism is due to micro-sheets at low load levels and deformation units at higher load levels.
- no apparent strain-rate effect was noticed on the ultimate tensile strength, strain at failure and elastic modulus. For 10 mm/min tests, only the conclusion on the ultimate tensile strength is valid. The values calculated for such parameters are in very good agreement with those reported in literature.

This first approach has enlighten several challenges related to the material testing and has therefore established what focus must be followed in future investigations.

References

Apollinari, G., Brüning, O., Nakamoto, T., Rossi, L., 2017. High luminosity large hadron collider HL-LHC. arXiv preprint arXiv:1705.08830 .

Bertarelli, A., Carra, F., Cerutti, F., Dallocchio, A., Garlasche, M., Guinchard, M., Mariani, N., dos Santos, S.M., Peroni, L., Scapin, M., et al., 2013. Behaviour of advanced materials impacted by high energy particle beams, in: Journal of Physics: Conference Series, IOP Publishing. p. 012005.

Bertarelli, A., Dallocchio, A., Kurtyka, T., 2008. Dynamic response of rapidly heated cylindrical rods: longitudinal and flexural behavior. Journal of Applied Mechanics 75.

Carra, F., 2017. Thermomechanical response of advanced materials under quasi instantaneous heating. Ph.D. thesis. PhD Thesis, Politecnico di Torino, Italy.

CERN website, . The Large Hadron Collider — CERN. https://home.cern/science/accelerators/large-hadron-collider. (Accessed on 08/15/2020).

Chung, D., 2014. Interface-derived extraordinary viscous behavior of exfoliated graphite. Carbon 68, 646–652.

Chung, D., 2016. A review of exfoliated graphite. Journal of materials science 51, 554–568.

Dowell, M., Howard, R., 1986. Tensile and compressive properties of flexible graphite foils. Carbon 24, 311–323.

Gandhi, J., Pathak, A., 2012. Performance evaluation of thermal interface material for space applications, in: Applied Mechanics and Materials, Trans Tech Publ. pp. 135–141.

Gu, J., Leng, Y., Gao, Y., Liu, H., Kang, F., Shen, W., 2002. Fracture mechanism of flexible graphite sheets. Carbon 40, 2169–2176.

Jenkins, G., 1962. Analysis of the stress-strain relationships in reactor grade graphite. British Journal of Applied Physics 13, 30.

Kobayashi, M., Toda, H., Takeuchi, A., Uesugi, K., Suzuki, Y., 2012. Three-dimensional evaluation of the compression and recovery behavior in a flexible graphite sheet by synchrotron radiation microtomography. Materials characterization 69, 52–62.

Luo, X., Chung, D., 2000. Vibration damping using flexible graphite. Carbon 38, 1510–1512.

Marotta, E., Mazzuca, S.J., Norley, J., 2005. Thermal joint conductance for flexible graphite materials: analytical and experimental study. IEEE Transactions on Components and Packaging Technologies 28, 102–110.

Martin, C.T., Perillo-Marcone, A., Calviani, M., Gentini, L., Butcher, M., Muñoz Cobo, J.L., 2019. Experiment exposing refractory metals to impacts of 440 GeV/c proton beams for the future design of the cern antiproton production target: Experiment design and online results. Phys. Rev. Accel. Beams 22, 013401. URL: https://link.aps.org/doi/10.1103/PhysRevAccelBeams.22.013401, doi:10.1103/PhysRevAccelBeams.22.013401.

Martin, C.T., Perillo-Marcone, A., Calviani, M., Muñoz-Cobo, J.L., 2016. Cern antiproton target: Hydrocode analysis of its core material dynamic response under proton beam impact. Physical Review Accelerators and Beams 19, 073402.

Neograf Solutions, . Grafoil- flexible graphite for fluid sealing applications. https://neograf.com/grafoil-flexible-graphite/. (Accessed on 08/15/2020).

Nuiry, F.X., 2018. Design and construction of beam intercepting devices (including targets) at CERN. https://indico.cern.ch/event/719240/contributions/3054072/attachments/1678452/2696235/Targets_and_BIDs_at_CERN.pdf. (Accessed on 08/17/2020).

Scapin, M., 2013. Shock-wave and high strain-rate phenomena in matter: modeling and applications. Torino, Italia .

Schmidt, R., Assmann, R., Carlier, E., Dehning, B., Denz, R., Goddard, B., Holzer, E., Kain, V., Puccio, B., Todd, B., et al., 2006. Protection of the cern large hadron collider. New Journal of Physics 8, 290.

SGL Carbon, . Smart Solutions in Graphites & Fiber Composites — SGL Carbon. https://www.sglcarbon.com/en/. (Accessed on 08/13/2020).

Shane, J.H., Russell, R.J., Bochman, R.A., 1968. Flexible graphite material of expanded particles compressed together. US Patent 3,404,061.

Solfiti, E., Berto, F., 2020a. Mechanical properties of flexible graphite. Procedia Structural Integrity 25, 420–429.

Solfiti, E., Berto, F., 2020b. A review on thermophysical properties of flexible graphite. Procedia Structural Integrity 26, 187–198.

Toda, H., Tsubone, K., Shimizu, K., Uesugi, K., Takeuchi, A., Suzuki, Y., Nakazawa, M., Aoki, Y., Kobayashi, M., 2013. Compression and recovery micro-mechanisms in flexible graphite. Carbon 59, 184–191.

Xi, X., Chung, D., 2019. Electret, piezoelectret, dielectricity and piezoresistivity discovered in exfoliated-graphite-based flexible graphite, with applications in mechanical sensing and electric powering. Carbon 150, 531–548.

Zazula, J., Péraire, S., 1996. LHC beam dump design study; 1, simulation of energy deposition by particle cascades; implications for the dump core and beam sweeping system. Technical Report.

Zukas, J.A., 1990. High velocity impact dynamics. Wiley-Interscience.